



## Using simulations of the detector performance for enhanced image reconstruction in molecular imaging



Irène Buvat\*

*Imagerie Moléculaire In Vivo, UMR 1023 Inserm/CEA/Université Paris Sud - ERL 9218 CNRS, CEA-Service Hospitalier Frédéric Joliot, Université Paris Saclay, Orsay, France*

### ARTICLE INFO

Available online 27 November 2015

#### Keywords:

PET  
SPECT  
Image reconstruction  
Monte Carlo simulations  
System matrix

### ABSTRACT

In Emission Tomography images are reconstructed by solving an inverse problem: the three-dimensional activity map producing the signal observed by the gamma camera or the Positron Emission Tomography (PET) detector is estimated given a model of the imaging system response. This model gives the set of probabilities  $\mathbf{R}_{ij}$  that a  $\gamma$  or  $\beta^+$  emission occurring at point  $j$  in the volume of interest be detected in detection element  $i$ . Thorough modeling of this  $\mathbf{R}$  system matrix (SM) is essential for ensuring the most accurate possible estimate of the activity distribution within the object of interest. Thirty years from now, it was proposed to calculate the system matrix  $\mathbf{R}$  based on Monte Carlo simulations, as opposed to using analytical geometrical models, for increased accuracy. A lot of progress has been made since the initial idea and using simulations for enhanced SPECT and PET image reconstruction has become a reality. In this paper, we review the rationale for this approach, explain the advantages and limitations, the performance that can be achieved, and the challenges that remain to be solved.

© 2015 Elsevier B.V. All rights reserved.

### 1. Introduction

In Single Photon Emission Computed Tomography (SPECT) and Positron Emission Tomography (PET) molecular imaging, images are obtained by solving an inverse problem, that is by estimating the unknown  $\gamma$  or  $\beta^+$  radiotracer activity distribution that is best compatible with the measured data, given a model of the imaging system response function. In a discrete formalism, this corresponds to solving the following equation:

$$p = \mathbf{R}f \quad (1)$$

where  $p$  represents the projections or the sinograms arranged as a 1D vector,  $f$  is the activity distribution to be reconstructed also arranged as a 1D vector and  $\mathbf{R}$  is a 2D matrix, called the system matrix (SM), that describes how  $f$ , in the so-called “image space”, is transformed into  $p$  in the projection space. Each entry  $\mathbf{R}_{ij}$  represents the probability that a  $\gamma$  photon or a  $\beta^+$  particle emitted in voxel  $j$  of the object be detected in projection bin  $i$ . The quality of the reconstructed images is directly affected by the ability of the SM to accurately describe the response of the imaging system. For a long time, the entries of this SM have been calculated using a line

integral model accounting for a simplified description of the detection geometry [1,2]. Yet, this is an idealized model for emission tomography (ET), both from the geometric and the physics points of view. Indeed, the line integral model assumes that the observed flux of photons arriving in one bin of the detector is only due to activity along an infinitesimally narrow line, which is obviously a crude assumption in SPECT since this would assume a perfect collimation (no divergence, no spatial spread, no collimator penetration). This is approximate in PET as well since the line of response (LOR) defined by two crystals is actually a tube of response including many possible narrow LOR. Some more sophisticated geometrical analytical models have been proposed [3,4]. The simplified line integral or more sophisticated geometrical approximations also neglect some important physics aspects that are inherent to ET, including scatter and attenuation in the object under investigation, interactions within the collimator in SPECT, positron range in PET, or particle interactions within the detector crystals. For the reconstructed  $f$  activity distribution to accurately estimate the actual activity distribution, the SM should precisely reflect the real probability controlling the physical experiment, ideally including all physics and geometrical effects.

As soon as 1985, Floyd et al [5,6] suggested that a more realistic model of a SPECT acquisition be used for SM calculation and proposed to have that model established using Monte Carlo simulations. Indeed, at that time, Monte Carlo (MC) simulations were

\* Correspondence to: IMIV, UMR 1023 Inserm/CEA/Université Paris Sud - ERL 9218 CNRS, CEA/I2BM/SHFJ 4 place du Général Leclerc 91400 Orsay France. Tel.: +33 1 69 86 77 79; fax: +33 1 69 86 77 86.

E-mail address: [irene.buvat@u-psud.fr](mailto:irene.buvat@u-psud.fr)

already shown to accurately reproduce SPECT acquisitions and offered the possibility to account for many physical characteristics of the acquisition system (energy window setting, energy and spatial resolutions, radius of rotation defining the solid angles through which a given point in the object is seen by the detector) and for the object-dependent scattering medium in which the photons propagate and undergo scatter and attenuation. The implementation as proposed by Floyd et al was only in 2D, ie reconstruction of a 2D image including 1,026 voxels, from a tomographic acquisition of 180 views of 64 measurements, for computation time reasons. The same idea of MC-based SM calculation was proposed for PET in 1988 [7] with a complete modeling of Compton scattering, detection efficiency, attenuation, positron range and non-collinearity of the annihilation photons, still in 2D. The extension to fully 3D reconstruction was introduced in 2004 for Tc-99m SPECT by Lazaro et al. [8,9], with MC calculation of the SM modeling scatter and attenuation in the object and accounting for the detector response function (DRF). This initial report showed a definite advantage of iterative reconstruction using the MC-based SM compared to iterative reconstruction accounting for attenuation, scatter and DRF using an analytical SM model (Fig. 1). In PET, the use of a MC-calculated SM in fully 3D was reported first for small animal imaging [10], modeling the geometric response of the system and photon scattering within the detector. Based on these seminal studies that demonstrated the feasibility of accurate SM calculation based on comprehensive 3D MC modeling of object and/or detector features, many investigators have extended the original ideas, evaluating the benefit of making the SM more accurate, and proposing solutions to overcome the hurdles associated with the practical implementation of this approach.

To give an overview of the importance of simulations for accurate image reconstruction in PET and SPECT, the outline of the paper will be as follows. Section 2 will explain how the simulation of the detector performance and of the whole imaging settings can offer an elegant approach for quantitative image reconstruction in ET. Section 3 will present the challenges associated with this approach, while Section 4 will discuss the applications investigated so far and associated performance, before drawing some conclusions.

## 2. How can simulations contribute to accurate image reconstruction?

### 2.1. Deriving SM using simulations

SM calculation requires each  $R_{ij}$  entry of the SM to be estimated. This probability that a  $\gamma$  photon or a positron emitted in voxel  $j$  of the object be detected in projection bin  $i$  depends not only on the type of particle, and on the detector features, but also on the object properties, which impact the interactions that

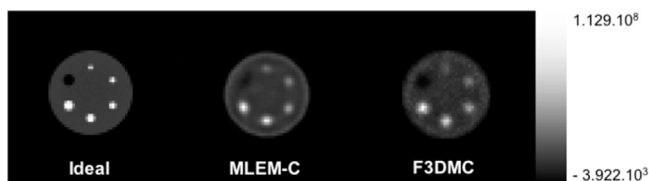


Fig. 1. Very first study demonstrating the feasibility of 3D SPECT reconstruction using a system matrix (SM) calculated using Monte Carlo (MC) simulations. Qualitative comparison between a simulated SPECT image reconstructed using MLEM involving either an analytical SM including attenuation and point spread function correction applied on scatter corrected projections (MLEM-C) or using a SM estimated using MC simulation (F3DMC). The cylindrical inserts are less distorted using the Monte Carlo SM. Adapted from ref [9] in which all reconstruction details can be found.

particles emitted in the object will undergo. Therefore, for a given acquisition protocol involving a specific radiotracer and detector, a different  $R$  should ideally be calculated for each patient (or animal). The major advantage of using a simulation approach to calculate  $R$  is that every phenomenon involved in the image formation process can a priori be accounted for in the reconstruction as long as it can be modeled using simulations. The simulation-based SM calculation is especially appealing for modeling phenomena for which there is no simple analytical model, such as those governed by a succession of probability laws, or by specific detector or patient features. Simulations can also be extremely useful for determining the parameters of an analytical model that is then used to produce the SM. In that latter case, SM entries are not directly derived from simulations, but they are set via a model that is itself parameterized using simulations. To distinguish between these two approaches, we will call these latter SM as MC-driven-SM, while MC-SM will refer to matrices for which each entry is directly derived from simulations.

A SM can also be factorized into a product of independent submatrices, each describing an aspect of image formation (detector geometrical component, particle interactions within the object, particle interactions within the detector, positron range in PET, etc) [11]. This reduces the size of the matrices to be stored and allows for an independent computation of each contribution using the most appropriate model. In that approach, only one or some components can be calculated using MC simulations, while others can be accurately set analytically [12]. This decomposition of the SM will be called factorized SM in the following.

### 2.2. Effects modeled in simulation-based SM matrices

Simulations are used either to comprehensively model the detector response function (DRF), or to model the probability of particle interactions within the patient, or both.

In SPECT, Floyd et al initially modeled the scatter and attenuation occurring in the object or patient to derive an MC-SM (2D approach), already demonstrating the qualitative and quantitative gain brought by the method [5,6] in 2D. Then, the same group included the DRF in their model. In SPECT, the DRF depends on the distance between the source and the collimator. This distance dependence is due to solid angles defined by the collimator holes and results in a position dependent non-symmetry in the reconstructed image point response. Modeling this effect in the MC-SM led to an impressive improvement in the spatial resolution of the reconstructed images (FWHM of a line spread function reduced by a factor of  $\sim 2$ , [13]). This effect is now almost systematically compensated for in SPECT iterative reconstruction using an analytical (as opposed to a MC) model [14] but this early work demonstrated the importance of accounting for the DRF in SPECT reconstruction. The DRF consists of a geometric component, a septal penetration component and a collimator scatter component. The geometric response can be easily modeled analytically based on the detailed geometric specifications of the hole and septa of the collimator and is the dominating component for low energy radionuclides. The septal penetration and collimator scatter response are more difficult to model and should not be neglected for radionuclides emitting medium or high-energy photons, such as I-123, In-111, Ga-67 and I-131. Simulations are then extremely helpful to account for these components. They can be used to generate a table of DRF as a function of the distance between the source and the detector for a MC-driven-SM approach (eg, [15–18]) or to directly calculate the MC-SM entries (eg, [19]).

In PET, the very first attempts of MC-SM calculation included the detailed modeling of photon interactions within the detector (Compton scattering, detection efficiency, attenuation), the positron range and the non-collinearity of the annihilation photons, in 2D

brain PET [7], but did not model the interactions within the object. The MC modeling of the detector response was described in small animal imaging [10,20,21] in 3D, but again, the interactions within the object were not accounted for. A complete MC modeling including the interactions both in the various components of the detector and in object was described in Shokouhi et al [22] for small animal PET, using a simplified model for the attenuation medium (homogenous water cylinder 35.5 mm in diameter and 20.23 mm in length) in C-11 imaging. A few studies also modeled the positron range (eg, [23–25]). Although the modeling of the positron range can be ignored for standard radionuclides in clinical scans (such as F-18, C-11), it becomes especially important for emitters with a large positron maximum energy, such as Rb-82 ( $E_{\max}=3.15$  MeV, positron range  $\sim 2.6$  mm in water), Ga-68 ( $E_{\max}=1.9$  MeV, positron range  $\sim 1.35$  mm in water), Cu-60 ( $E_{\max}=3.77$  MeV, positron range  $\sim 3.1$  mm in water), and Cu-61 ( $E_{\max}=1.21$  MeV, positron range  $\sim 1.3$  mm in water), in small animal imaging where a submillimetric spatial resolution is targeted. It can be modeled either in a MC-SM approach, or MC simulations can be used to determine the blurring effect due to positron range for a given radionuclide that is then incorporated in a factorized MC-driven-SM in which other components are modeled analytically [23,24]. To avoid the computational burden associated with an MC-SM estimate (see Section 3.1), an MC-driven-SM was also used to accurately model the inter-crystal scattering and penetration and the intra-crystal count distribution in small animal PET [26] and in human PET [27] (Fig. 2). A factorized SM involving a MC simulated component for describing the detector response was also reported for clinical PET [28] and for a small animal PET scanner involving planar rotating detector heads [12].

In ET, the classical use of a grid of voxels to describe the reconstructed image is not the only possible representation. In particular this description does not fully exploit the symmetrical arrangement of PET detectors along a ring. Alternative representations include the use of polar voxels [29,30], spherically symmetric basis functions also known as blobs [31–34] or natural pixels [35]. In the spherically symmetric basis functions and natural pixel representations, the object is represented by a sum of smoothed functions. The SM corresponding to these various representations is not necessarily easy to calculate for a realistic detector geometry. MC simulations alleviate this problem, as the SM elements can be easily determined for any pixel representation. In PET, natural pixels values have been calculated using MC simulations [35] in 2D, and Cabello et al presented a detailed comparison of the reconstructed image properties as a function of whether the MC-SM calculation was based on cubic voxels, polar voxels and spherically symmetric basis functions [36].

### 3. Challenges for simulation-based tomographic reconstruction

Although theoretically extremely appealing, the SM calculation based on MC simulations faces significant challenges: the computational time required to obtain a statistically robust estimate of each  $R_{ij}$  entry, the storage of the SM, and the computational time needed for reconstructing data based on a large and non-sparse SM matrix. Several strategies have been suggested to address these challenges and make MC-based calculation of SM tractable.

#### 3.1. Computational time issues for SM calculation and SM statistical quality

When calculating each  $R_{ij}$  entry using MC simulations, the statistical quality of  $R_{ij}$  will depend on how many events were used to estimate its value. The greater the number of events, the better the statistical quality of  $R_{ij}$  and the more accurate the reconstructed image (Fig. 3). Obtaining an  $R_{ij}$  estimate with a satisfactory statistical quality might not be an issue when there are many events emitted in voxel  $j$  that are detected in detector bin  $i$ , but when rare particle histories link  $i$  and  $j$ , then numerous particles will have to be simulated to accurately estimate  $R_{ij}$ . Simulations involving a large number of particle histories are thus needed to get a robust estimate of the many  $R_{ij}$ , including entries with a low probability.

A first approach that can be used to alleviate the computational burden associated with MC-based calculation of the SM is to develop faster and dedicated MC simulators. The MC simulation codes classically used in ET, such as, for instance, Geant4 [37], GATE [38,39], Simset [40], SIMIND [41], or PeneloPET [42], are not optimized for SM calculation in terms of computational efficiency. When the only purpose of a MC simulation code is to calculate the SM, simplifications can be made and the code can become far more efficient. Examples have been described in SPECT (eg [43–45]) and in PET (eg, [21,46,47]).

Another approach is to take advantage of the scanner symmetries to increase the statistical quality of each entry, and reduce the storage space needed [10,36]. Indeed, due to the scanner symmetries, if omitting the object-related effects (that are not symmetrical in general), several  $R_{ij}$  are theoretically identical. In PET, the detector presents axial and in-plane reflection symmetries (eg, [21,46,48,49]). Ignoring edge and block effects, one can also assume some translational symmetry [46]. Accounting for these symmetries, the number of SM entries can be reduced by one or two orders of magnitude (eg, [46,48,49]). Using the same idea, it has also been proposed to use so-called quasi-symmetries,

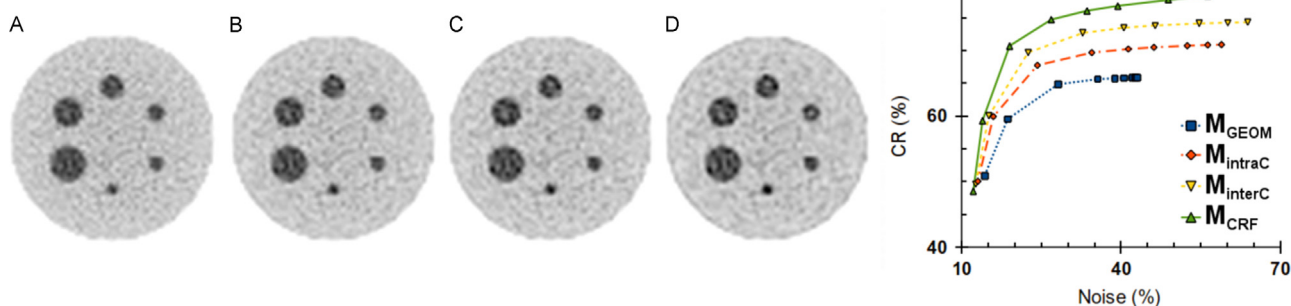


**Fig. 2.** Impact of modeling the intra-crystal count distribution (intraC: B), or the inter-crystal scattering and penetration (interC: C), or both (CRF: D) in the SM used for PET reconstruction instead of using a geometric model linking the center of two crystals to define the LOR (GEOM: A). The most accurate SM (D) yields the highest contrast recovery (CR) as illustrated in the graph corresponding to measures performed in the smallest sphere of this simulated phantom. Adapted from Ref. [27] in which all reconstruction details can be found.

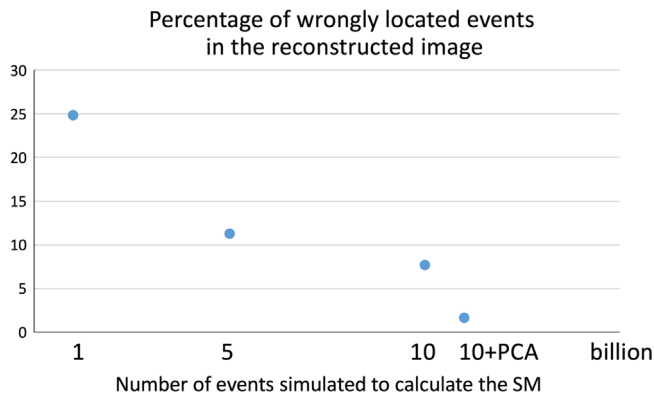


**Fig. 3.** Impact of the number of events simulated to estimate the SM on the percentage of events located at a wrong position in the reconstructed images of a simulated phantom. The impact of filtering the SM using a Principal Component Analysis is also shown (10+PCA). Phantom and reconstruction details are given in ref [9].

ie to assume that SM elements that are not strictly identical can be set to the same value [46]. The reduction in the number of SM entries to be estimated then depends on the definition of “nearly identical” and on the desired accuracy in the final reconstructed images.

The number of scanner symmetries that can be taken advantage of is limited by the shape of the voxel and the reconstruction grid definition. The conventional cubic voxel (ie a Cartesian grid) discretization limits the number of symmetries that can be used. Other discretizations, such as the use of polar voxels or blobs discussed above, increase the number of possible symmetries ([50,51] in SPECT, [36] in PET), thus reducing the number of  $R_{ij}$  matrix to be estimated, hence the computational cost.

The main limitation of this approach is that symmetries or quasi-symmetries only apply to detector-related effects. The object under investigation (animal or patient) does not present symmetries. As a result, the object-related effects have to be dealt with before reconstruction, or using a factorized SM in which the components involving symmetries and the others are separated.

The SM can be filtered in some way, to reduce the noise affecting each  $R_{ij}$  entry. Several filtering methods have been suggested. One consists in using a threshold in probability so that each  $R_{ij}$  lower than that threshold is set to zero, ie the corresponding probability of occurrence of that event is neglected. A single threshold can be set for the entire SM ([12,52–54]), or for each LOR and associated channel of response [46], and the level of filtering can be tuned by changing the threshold. Another approach consists in using a Principal Component Analysis for SM filtering [9], where the number of principal components determines the strength of the noise removal (Fig. 3).

Last, approximations can be made to speed up the SM calculation using a simplified model of activity distribution within each voxel (for instance, a point source at the center of a voxel instead of a uniform activity distribution) [55].

### 3.2. Matrix storage

In 3D imaging, the number of matrix elements is extremely high, as it is equal to the number of detector elements over all projection lines (or LOR in PET) times the number of voxels to be reconstructed. As an examples, in the eXplore Vista-DR (GE) small animal PET scanner with an axial field of view (FOV) of 4.6 cm and a transaxial FOV of 6.8 cm, the number of LOR is greater than 10 millions. When reconstructing a  $175 \times 175 \times 62$  voxel volume in that scanner, the number of entries in the SM will be greater than  $10^{13}$  [46]. The resulting SM would therefore require several TBytes

to be stored, which is practically not feasible on a conventional workstation. In clinical PET and SPECT, the number of entries in the SM is of the same order. Yet, many of the SM entries are actually null. Indeed, every LOR in PET can detect coincidences from only a small portion of the FOV. The voxels “feeding” a given LOR are sometimes called channel of response (CHORD) [56] for that LOR. Similarly, in SPECT, a projection bin only detects events coming from a small region of the gamma camera FOV. Therefore, the SM is extremely sparse and the number of non-null matrix elements to be stored is considerably reduced. Accounting for the detector geometry only, typically less than 10% of SM elements are non-zero. Sparse matrix techniques can then be used to store the SM [57]. However, this high sparsity is only observed when ignoring scatter events. Indeed, because of scatter, a particle emitted in any voxel of the FOV can be detected in almost any detector element. Accounting for object scatter in the SM therefore considerably decreases the sparseness of the SM, making matrix storage and computation time severe hurdles. Other solutions have then to be found to make the use of MC-based SM tractable, one of these being the setting of low  $R_{ij}$  values to zero, as explained in Section 3.1.

When the SM is small enough (up to several GBytes, [58]), it can be computed once for a detector geometry and stored on disk in a sparse matrix format to be subsequently used for any reconstruction involving the same detector set-up. Yet, this precalculation is only appropriate for object-independent SM, hence reducing the potential of the MC-based SM approach. Various strategies can be used to handle the storage burden, including using a database for gathering all values needed to derive SM entries [10], taking advantage of the detector symmetries [36,46,54], or adjusting the sampling as a function of the SM component [48]. The factorization of the matrix into independent components also helps in handling the large amount of data [12]. Some SM can even be kept in the computer random access memory (RAM) for increasing the reconstruction speed [46].

Alternatively, some MC-SM components can be calculated on the fly, avoiding the need for storing the whole SM matrix on disk (e.g., [24,59,60]), based on realistic approximations, such as the low frequency nature of the spatial distribution of scatter events for instance.

### 3.3. Reconstruction time

As discussed above, SM incorporating a detailed description of all detector and object effects are no longer sparse. In addition, these intricate SM are often poorly conditioned, ie difficult to invert. This has two consequences: the ill-conditioning leads to a slower convergence rate, and the low-sparsity yields long computation time at each iteration of the iterative reconstruction algorithm. All together, this increases the reconstruction time [12]. An elegant approach to deal with the increased computation time produced by complex SM is a two-level reconstruction algorithm, in which both a simplified SM and an accurate SM are used alternatively [24]. The simplified SM ensures efficient computation while the accurate SM retains the accuracy of the final solution. The algorithm consists in compensating for the error introduced by the simplified SM by introducing a correction term. In that approach, the accurate SM is not used at each iteration, so that computation time is saved. The resulting images are still very close to those obtained when always using the complex SM, but the reconstruction time is reduced by an order of magnitude.

During reconstruction, any entry of the SM needs to be accessed repeatedly. From that point of view, it is thus advantageous to have the SM stored in the RAM, instead of calculating the SM elements on the fly.

## 4. Applications

The use of MC-based SM has been reported in SPECT and PET, both for preclinical and clinical applications. The robustness of the approach with respect to the number of events used to produce the SM and to possible errors in SM modeling has also been investigated and the main results are summarized here.

### 4.1. Performance achieved with reconstruction involving an MC-based SM

In pinhole Tc-99m SPECT, the MC-SM reconstruction led to results very similar to those obtained with an SM estimated using an analytical approach combined with experimental measurements of the intrinsic detector response using a pencil beam [58]. This latter SM was faster to create and handled the projection noise better than the MC-SM, but the MC-SM avoided the tedious experimental characterization of the camera response, so each approach had its own advantages/drawbacks with similar performance. In parallel hole Tc-99m SPECT, the use of an MC-SM in which all detector and object-dependent effects were accurately modeled was also shown to significantly improve absolute activity quantitation and spatial resolution with respect to a MLEM reconstruction approach with associated scatter correction, attenuation correction, and compensation for the depth-dependent point spread function [9].

In I-131 SPECT, the importance of accounting for septal penetration by modeling it in a MC-SM was clearly demonstrated in Liu et al. [19].

In F-18-FDG small animal PET, the use of an MC-SM modeling the positron range, crystal penetration and inter-crystal scatter led to only slight improvement in terms of spatial resolution and contrast with respect to SM calculated using geometrical models only [47].

In F-18-FDG whole body PET, the MC-SM significantly improved the contrast recovery in hot and small spheres with respect to a multiray Siddon projector [54], but these results were obtained without any scattering / attenuation in the object. A detailed MC-based modeling of crystal photon interactions in the SM significantly improved the stationarity of the spatial resolution in the reconstructed image [27] (Fig. 4), as well as the contrast (Fig. 5).

Based on the literature, the applications that benefit the most from MC-based SM are those for which simplified SM are coarse approximations of the real imaging system response. These include all SPECT applications involving isotopes that significantly interact with the collimator through scatter and undergo septal penetration such as I-123 or I-131 (e.g., [19]). In PET, so-called dirty

isotopes, involving a complex decay scheme, such as I-124 [25], and isotopes for which the mean free-path in water is high with respect to F-18, also benefit the most from MC or MC-driven SM.

Yet, the gain in accuracy due to the thoroughly computed MC-based SM can be mitigated by the statistical noise affecting the SM matrix and a trade-off has to be found between the level of complexity modeled in the SM and the statistical robustness of its entries [25]. For instance, in I-124 PET mice imaging, quantitative accuracy was easier to achieve by modeling a uniform object attenuation medium, instead of accounting for its true heterogeneity, as this would require a huge computational effort to soundly estimate each SM entry [25].

### 4.2. Impact of the noise present in the SM

The impact of the noise affecting the SM entries has been studied in several reports. It has been shown that the convergence rate of the reconstruction algorithm towards the true activity values is significantly faster when the number of events used to produce the SM is increased [22], ie when the SM entries are less noisy. It was also found that the impact of noise in the SM depended on the iterative reconstruction scheme and on the number of iterations: the greater the number of iterations, the higher the effect of noise in the SM [52]. As expected, SM generated using a higher number of events produce images with less artifacts and higher signal to noise ratios than those obtained with an SM derived from less simulated events [9,12,52,53] (Fig. 3). PCA filtering of the SM also improved the reconstructed image accuracy (Fig. 3) and the signal to noise ratio (SNR) [9] while the impact of a threshold applied on the SM to prune low probability values was not easily predictable: some thresholding can actually improve the SNR in the reconstructed images [50] but can also reduce image accuracy [12].

The statistical quality of the SM can be estimated using a Relative Mean Error (RME) defined as follows:

$$\text{RME} = (\sum_{ij} n_{ij}^{-1/2}) / N \quad (2)$$

where  $n_{ij}$  is the number of events originating from voxel  $j$  and detected in detector bin  $i$  used for the SM calculation and  $N$  is the number of non-zero entries in the SM [10]. RME is a global figure of merit however and fails to reflect local inaccuracies in the SM [53].

A theoretical study [61] actually established a link between the errors present in the SM and the errors in the reconstructed images, making it possible to predict how many events should be simulated for SM calculation to ensure that the artefacts in the reconstructed images caused by statistical errors in the SM are small compared to the statistical Poisson noise in the measured projections. They showed that the total number of detected events in the forward projection should be more than  $1/a$  times the total number of

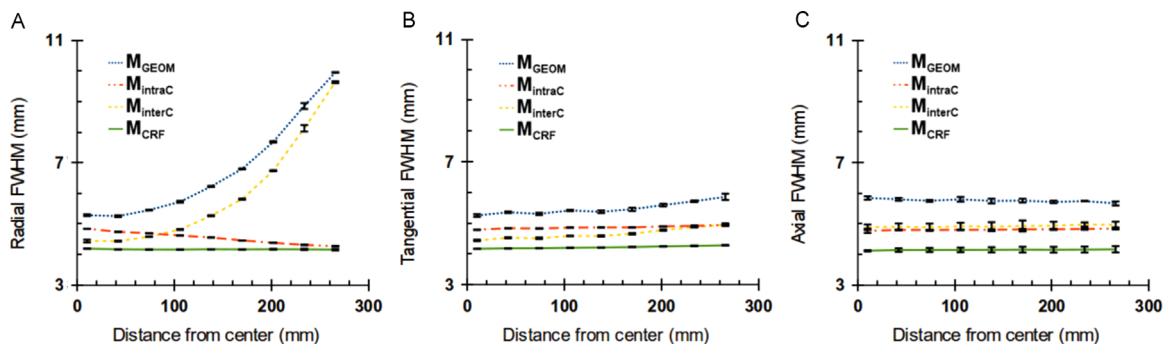


**Fig. 4.** Impact of modeling the intra-crystal count distribution (intraC), or the inter-crystal scattering and penetration (interC), or both (CRF) in the SM used for PET reconstruction instead of using a geometric model linking the centers of two crystals to define the LOR (GEOM) on the stationarity of the spatial resolution in the reconstructed images. The most accurate SM (CRF) yields a stationary spatial resolution in all directions (A: Radial, B: Tangential and C: Axial). Adapted from Ref. [27] in which all reconstruction details can be found.

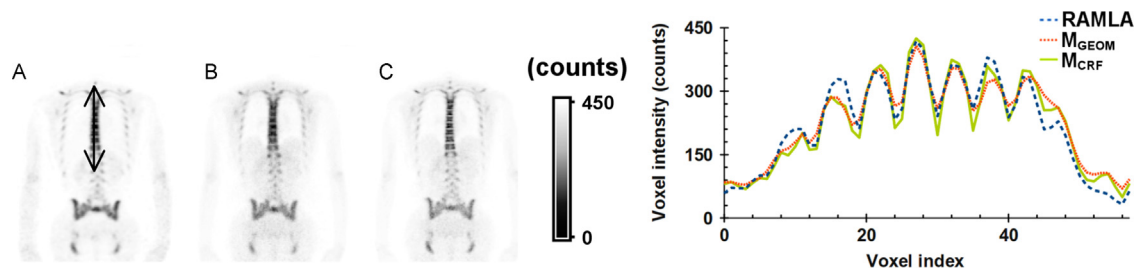


**Fig. 5.** Impact of modeling the intra-crystal count distribution and the inter-crystal scattering and penetration (C: CRF) in the SM used for PET Ordinary Poisson -OSEM reconstruction instead of using a geometric model linking the centers of two crystals to define the LOR (B: GEOM) shown on clinical images. The image provided by the manufacturer using a RAMLA algorithm without any detailed modeling of interactions in the detector crystal is also shown (A). The benefit of refined modeling of the interactions in the crystal clearly appears along the spine through which profiles have been drawn (right). Adapted from Ref. [27] in which all reconstruction details can be found.

detected events in the data set, where  $a$  is a user-defined tolerance factor, typically 0.01. This rule appears appropriate when the noise level is low enough in the projection data, but at high noise level, this theoretical derivation does not apply, as it is based on a linear approximation (first-order Taylor series) that does not match well the nonlinear properties of iterative reconstruction.

#### 4.3. Impact of modeling errors in the SM

Although the MC approach has the potential to produce a highly accurate description of the imaging system response for a given object, the quality of this description will depend on how well the detector and the object specifications are modeled. For instance, in SPECT, even small discrepancies between the collimator specifications provided by the manufacturer and the actual collimator features can yield significant differences between measured and simulated data. Although several articles deal with the impact of statistical errors in the system matrices (cf Section 4.2), to the best of our knowledge, few reports extensively studied the impact of systematic errors in the SM model. For instance, the voxel grid used for the SM calculation can be slightly misaligned with respect to that corresponding to the measured activity and attenuation maps. In human SPECT, small misalignments ( $\sim 2$  mm) did not impact the reconstructed images much, but misalignments greater than 5 mm would produce strong artifacts [9].

## 5. Conclusion

MC-based SM allows for a very accurate modeling of the imaging response system, possibly accounting for most detector and object-related effects. Yet, the computational burden associated with this approach has limited its widespread application so far. A convenient approach to make it tractable is to factorize the SM into different detector and object-related components, and to limit the MC calculations only to those effects that cannot be precisely modeled analytically. Another practical approach is to parameterize an analytical description of the SM based on MC calculations. Using different SM along the iterative reconstruction process to retain the accuracy of MC-SM in acceptable computation time is also an option. MC-based SM might be the only method to achieve accurate quantification for radiotracers involving radionuclides with a complex decay scheme, for detectors with a complicated geometry, or for making the most of what SPECT and PET can offer. Efforts should then be pursued to facilitate its implementation and take full advantage of its high potential. The rapid evolution of computational resource will certainly contribute to the more systematic implementation of MC-based reconstruction, in which both the object and the detector particularities will be more systematically introduced. When

object-dependent effects are modeled in the MC-based reconstruction, it can even be viewed as a component of personalized medicine, as image reconstruction then fully incorporates the specific patient characteristics.

## References

- [1] R.L. Siddon, *Medical Physics* 12 (1985) 252.
- [2] G.T. Herman, L.B. Meyer, *IEEE Transactions on Medical Imaging* 12 (1993) 600.
- [3] A. Terstegge, S. Weber, H. Herzog, H.W. Muller-Gartner, H. Halling. *IEEE Nucl. Sci. Symp. Med. Imaging Conf. Rec.*, 3, 1997, p. 1603.
- [4] J.J. Scheins, F. Boschen, H. Herzog, *IEEE Transactions on Medical Imaging* 25 (2006) 1363.
- [5] C.E. Floyd, R.J. Jaszczyk, R.E. Coleman, *IEEE Transactions on Nuclear Science* 32 (1985) 779.
- [6] C.E. Floyd, R.J. Jaszczyk, K.L. Greer, R.E. Coleman, *Journal of Nuclear Medicine* 27 (1986) 1577.
- [7] E. Veklerov, J. Llacer, J. E. Hoffman, *IEEE Transactions on Nuclear Science* 35 (1988) 603.
- [8] D. Lazaro, V. Breton, I. Buvat, *Nuclear Instruments and Methods in Physics Research Section A* 527 (2004) 195.
- [9] D. Lazaro, Z. El Bitar, V. Breton, D. Hill, I. Buvat, *Physics in Medicine and Biology* 50 (2005) 3739.
- [10] M. Rafecas, B. Mosler, M. Dietz, M. Pögl, A. Stamatakis, D.P. McElroy, S.I. Ziegler, *IEEE Transactions on Nuclear Science* 51 (2004) 2597.
- [11] J. Qi, R.M. Leahy, S.R. Cherry, A. Chatzioannou, T.H. Farquhar, *Physics in Medicine and Biology* 43 (1998) 1001.
- [12] M. Cecchetti, S. Moehrs, N. Belcari, A. Del Guerra, *Physics in Medicine and Biology* 58 (2013) 6713.
- [13] C.E. Floyd, R.J. Jaszczyk, S.H. Manglos, R.E. Coleman, *IEEE Transactions on Nuclear Science* 35 (1988) 784.
- [14] E.C. Frey, B.M.W. Tsui, *Quantitative Analysis in Nuclear Medicine Imaging*, Springer, Singapore (2006), p. 141.
- [15] M. Ljungberg, K. Sjögreen, X. Liu, E. Frey, Y. Dewaraja, S.E. Strand, *Journal of Nuclear Medicine* 43 (2002) 1101.
- [16] B. He, Y. Du, X. Song, W.P. Segars, E.C. Frey, *Physics in Medicine and Biology* 50 (2005) 4169.
- [17] Y. Du, B.M.W. Tsui, E.C. Frey, *Physics in Medicine and Biology* 51 (2006) 1269.
- [18] S.C. Moore, J. Ouyang, M.A. Park, G. El Fakhri, *Nuclear Instruments and Methods in Physics Research Section A* 569 (2006) 472.
- [19] S. Liu, T.H. Farncombe, *IEEE Nucl. Sci. Symp. Med. Imaging Conf. Rec.* 5, 2007, pp. 3955.
- [20] G. Böning, B.J. Pichler, M. Rafecas, E. Lorenz, M. Schwaiger, S.I. Ziegler, *IEEE Transactions on Nuclear Science* 40 (2001) 805.
- [21] J.E. Ortuno, G. Kontaxakis, J.L. Rubio, P. Guerra, A. Santos, *Physics in Medicine and Biology* 55 (2010) 1833.
- [22] S. Shokouhi, P. Vaska, D.J. Schlyer, M. Purschke, C.L. Woody, S.P. Stoll, S. Southekal, A. Villanueva, *IEEE Nucl. Sci. Symp. Med. Imaging Conf. Rec.*, 6, 2004, pp. 3901.
- [23] A. Ruangma, B. Bai, J.S. Lewis, X. Sun, M.J. Welch, R. Leahy, R. Laforest, *Nuclear Medicine and Biology* 33 (2006) 217.
- [24] L. Fu, J. Qi, *Medical Physics* 37 (2010) 704.
- [25] M. Moreau, I. Buvat, L. Ammour, N. Chouin, F. Kraeber-Bodéré, M. Cherel, T. Carlier, *Physics in Medicine and Biology* 60 (2015) 2475.
- [26] S. Moehrs, M. Defrise, N. Belcari, A. Del Guerra, A. Bartoli, S. Fabbri, G. Zanetti, *Physics in Medicine and Biology* 53 (2008) 6925.
- [27] S. Stute, D. Benoit, A. Martineau, N. Rehfeld, I. Buvat, *Physics in Medicine and Biology* 56 (2011) 793.
- [28] A.M. Alessio, P.E. Kinahan, T.K. Lewellen, *IEEE Transactions on Medical Imaging* 25 (2006) 828.
- [29] K. Kearfott, *Journal of the American Statistical Association* 80 (1985) 26.
- [30] L. Kaufman, *IEEE Transactions on Medical Imaging* 6 (1987) 37.
- [31] S. Matej, R.M. Lewitt, *IEEE Transactions on Medical Imaging* 15 (1996) 68.

- [32] M.E. Daube-Witherspoon, S. Matej, J.S. Karp, R.M. Lewitt, IEEE Transactions on Nuclear Science 48 (2001) 24.
- [33] A. Andreyev, M. Defrise, C. Vanhove, IEEE Transactions on Nuclear Science 53 (2006) 2719.
- [34] A. Yendiki, J.A. Fessler, Physics in Medicine and Biology 49 (2004) 2157.
- [35] S. Vandenberghe, S. Staelens, C.L. Byrne, E.J. Soares, I. Lemahieu, S.J. Glick, Physics in Medicine and Biology 51 (2006) 3105.
- [36] J. Cabello, M. Rafecas, Physics in Medicine and Biology 57 (2012) 1759.
- [37] S. Agostinelli, et al., Nuclear Instruments and Methods in Physics Research Section A 506 (2003) 250.
- [38] S. Jan, et al., Physics in Medicine and Biology 49 (2004) 4543.
- [39] S. Jan, et al., Physics in Medicine and Biology 56 (2011) 881.
- [40] R.L. Harrison, S.D. Vannoy, D.R. Haynor, S.B. Gillipsie, M.S. Kaplan, T.K. Lewellen, In: Proceedings of the Conference Record, IEEE Nuclear Science Symposium and Medical Imaging Conference, San Francisco, (1993), pp. 1154.
- [41] M. Ljungberg, S.E. Strand, Computer Methods and Programs in Biomedicine 29 (1989) 257.
- [42] S. Espana S, J.L. Herraiz, E. Vicente, J.J. Vaquero, M. Desco, J.M. Udias, Physics in Medicine and Biology 54 (2009) 1723.
- [43] X. Song, W.P. Segars, Y. Du, B.M.W. Tsui, E.C. Frey EC, Physics in Medicine and Biology 50 (2005) 1791.
- [44] A. Cot, E. Jane, J. Sempau, C. Falcon, S. Bullich, J. Pavia, F. Calvino, D. Ros, IEEE Transactions on Nuclear Science 53 (2006) 198.
- [45] S. Staelens, T. de Wit, F. Beekman, Physics in Medicine and Biology 52 (2007) 3027.
- [46] J.L. Herraiz, S. Espana, J.J. Vaquero, M. Desco, J.M. Udias, Physics in Medicine and Biology 51 (2006) 4547.
- [47] P. Aguiar, M. Rafecas, J.E. Ortuno, G. Kontaxakis, A. Santos, J. Pavia, D. Ros, Medical Physics 37 (2010) 5691.
- [48] V.Y. Panin, F. Kehren, H. Rothfuss, D. Hu, C. Michel, M.E. Casey, IEEE Transactions on Nuclear Science 53 (2006) 152.
- [49] J.J. Scheins, H. Herzog, N.J. Shah, IEEE Transactions on Medical Imaging 30 (2011) 879.
- [50] T. Hebert, R. Leahy, M. Singh, IEEE Transactions on Nuclear Science 35 (1988) 615.
- [51] V. Israel-Jost, P. Choquet, S. Salmon, C. Blondet, E. Sonnendrücker, A. Constantinesco, IEEE Transactions on Medical Imaging 25 (2006) 158.
- [52] M. Rafecas, G. Böning, B.J. Pichler, E. Lorenz, M. Schwaiger, S.I. Ziegler, IEEE Transactions on Nuclear Science 51 (2004) 149.
- [53] F.R. Rannou, A.F. Chatzioannou, IEEE Nucl. Sci. Symp. Med. Imaging Conf. Rec., 6, 2004, pp. 3433.
- [54] L. Zhang, S. Staelens, R.V. Holen, J.D. Beenhouwer, J. Verhaeghe, I. Kawrakow, S. Vandenberghe, Medical Physics 37 (2010) 3667.
- [55] E.N. Gimenez, E. Nacher, M. Gimenez, J.M. Benlloch, M. Rafecas, Nuclear Instruments and Methods in Physics Research Section A 569 (2006) 346.
- [56] C. Michel, et al., IEEE Nucl. Sci. Symp. Med. Imaging Conf. Rec., 15, 2000, pp. 207.
- [57] C.A. Johnson, Y. Yan, R.E. Carson, R.L. Martino, M.E. Daube-Witherspoon, IEEE Transactions on Nuclear Science 42 (1995) 1223.
- [58] P. Aguiar, F. Pino, J. Silva-Rodriguez, J. Pavia, D. Ros, A. Ruibal, Z. El Bitar, Medical Physics 41 (2014) 032501.
- [59] H. Kudrolli, W. Worstell, V. Zavarzin, IEEE Transactions on Nuclear Science 49 (2002) 124.
- [60] F.J. Beekman, H.W.A.M. de Jong, S. van Geloven, IEEE Transactions on Medical Imaging 21 (2002) 867.
- [61] J. Qi, R.H. Huesman, Physics in Medicine and Biology 50 (2005) 3297.